Title
Disparate Catalytic Scaffolds for Atroposelective Cyclodehydration

Journal
Journal of the American Chemical Society, 141(16)

ISSN
0002-7863

Authors
Kwon, Yongseok
Li, Junqi
Reid, Jolene P
et al.

Publication Date
2019-04-24

DOI
10.1021/jacs.9b01911

Peer reviewed

HHS Public Access

Author manuscript

J Am Chem Soc. Author manuscript; available in PMC 2020 April 24.

Published in final edited form as:

J Am Chem Soc. 2019 April 24; 141(16): 6698–6705. doi:10.1021/jacs.9b01911.

Disparate Catalytic Scaffolds for Atroposelective Cyclodehydration

Yongseok Kwon[†], **Junqi Li**[†,‡], **Jolene P. Reid**[#], **Jennifer M. Crawford**[#], **Roxane Jacob**[‡], **Matthew S. Sigman**[*,#], **F. Dean Toste**[*,‡], and **Scott J. Miller**[*,†]

[†]Department of Chemistry, Yale University, New Haven, Connecticut 06520-8107, United States

[‡]Department of Chemistry, University of California, Berkeley, California 94720, United States

[#]Department of Chemistry, University of Utah, 315 South 1400 East, Salt Lake City, Utah 84112, United States

Abstract

Catalysts that control stereochemistry are prized tools in chemical synthesis. When an effective catalyst is found, it is often explored for other types of reactions, frequently under the auspices of different mechanisms. As successes mount, a unique catalyst scaffold may become viewed as "privileged". However, the mechanistic hallmarks of privileged catalysts are not easily enumerated, nor readily generalized to genuinely different classes of reactions or substrates. We explored the concept of scaffold uniqueness with two catalyst types for an unusual atropisomer-selective cyclodehydration: (a) C_2-symmetric chiral phosphoric acids, and (b) phosphothreonine-embedded, peptidic phosphoric acids. Pragmatically, both catalyst scaffolds proved fertile for enantioselective/atroposelective cyclodehydrations. Mechanistic studies revealed that the determinants of often equivalent and high atroposelectivity are different for the two catalyst classes. A data-descriptive classification of these asymmetric catalysts reveals an increasingly broad set of catalyst chemotypes, operating with different mechanistic features, that creates new opportunities for broad and complementary application of catalyst scaffolds in diverse substrate space.

Graphical Abstract

[*]**Corresponding Author:** matt.sigman@utah.edu, fdtoste@berkeley.edu, scott.miller@yale.edu.

ASSOCIATED CONTENT

Supporting Information

The Supporting Information is available free of charge on the ACS Publications website.

Experimental details, procedures, compound characterization data, computational details, and copies of ^{1}H and ^{13}C NMR spectra of new compounds (PDF)

X-ray crystallographic data for **2a** (CIF)

Notes

The authors declare no competing financial interest.

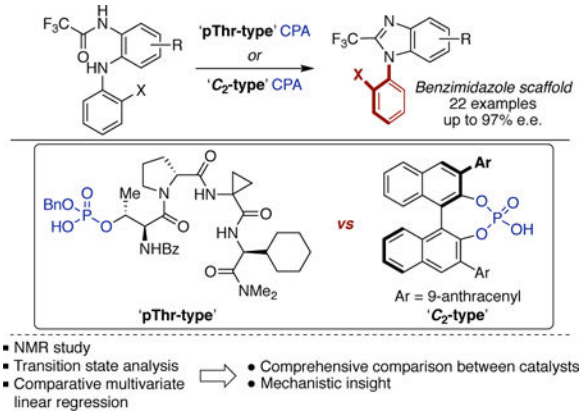

INTRODUCTION

Chemists rarely know what type of catalyst will be well-suited to a new substrate class or reaction type *a priori*. The closer to precedent the desired transformation is, the more readily chemists can predict an effective catalyst scaffold.[1,2] To that extent, a few principles have emerged to guide chemists in uncharted reaction territory.[3] Among these, the evaluation of catalysts deemed "privileged" is a common starting point for the consideration of a catalyst chemotype.[4,5] This leads to questions: How unique are privileged catalysts? To what extent are privileged catalysts exclusively matched for a number of reactions proceeding through a common mode of activation? Can a different catalyst scaffold also achieve high selectivity for the same reactions through alternative modes of action? In addition, do privileged catalysts remain effective beyond simple substrates, or can there be a different catalyst scaffold that offers complementarity when substrates become more complex? Episodic disclosures of different catalysts classes for the same transformation, on the same substrate, exist in several widely-explored asymmetric reactions such as the catalytic hydrogenation,[6] aldol[7] and Diels-Alder reactions[8] (Scheme 1). Harnessing different catalyst designs for effective enantiocontrol is therefore possible, but direct comparative studies of the substrate preferences, and their different mechanistic underpinnings has been difficult to achieve rigorously and retrospectively, given the multiple laboratories and diverse reaction conditions often engaged. The present study confronts these questions in an experimentally and computationally driven manner through the comparative study of two distinct catalyst classes that are effective for the enantioselective and atropisomer-selective cyclodehydration of *o*-sub-stituted aniline derivatives to deliver optically enriched benzimidazoles,[9] *N*-heterocycles of high interest in drug-like molecules[10] as shown in Figure 1c.

The two catalyst classes hail from disparate realms of the asymmetric catalysis landscape. One catalyst class, C_2-symmetric chiral phosphoric acids derived from BINOL (C_2-type),[11] is widely accepted as a privileged scaffold, which has been effectively utilized in an exceedingly large number of reports (Figure 1a).[12] The second class incorporates peptide-based phosphoric acids, inspired by the ubiquitous biochemically relevant moiety, phosphothreonine (pThr) as shown in Figure 1a. pThr is formed by enzymatic phosphorylation, resulting in numerous biochemical signal transduction cascades.[13] Interestingly, this motif is not to our knowledge known to play a catalytic role implicated in

bond formation or cleavage in any enzyme. Yet, pThr-based catalysts have recently been found to be effective for asymmetric reactions such as transfer hydrogenation[14] and the Baeyer-Villiger oxidation of cyclobutanones[15] (Figure 1b). Critically, in each case good selectivity was found for C_2-type-and peptide-based chiral phosphoric acids. In the case of Baeyer-Villiger oxidation, the pThr-type catalyst actually gives better selectivity than a canonical C_2-type catalyst with a functionalized substrate.

Detailed below is the experimental documentation that both C_2-type and pThr-type CPAs can catalyze a wide array of atroposelective cyclodehydrations in very high enantioselectivity. Challenging each catalyst class with a range of substrate types reveals not only intriguing strengths and weaknesses for each as a function of substrate, but perhaps even more curiously, high functional homology for other substrates. Catalyst and substrate structure-selectivity relationships (SSRs) and context dependent mechanistic studies point to subtle but a distinct set of control elements that lead to common selectivity outcomes in many cases.[16]

RESULTS AND DISCUSSION

Catalyst optimizations.

The context for this study is in the area of catalytic asymmetric synthesis of atropisomers, which is a relatively young subfield of asymmetric catalysis, with a variety of ap-proaches now reported,[17,18] including asymmetric cross-coupling[19] and dynamic kinetic resolutions.[20] Few catalytic atropisomer-selective methods target medicinally relevant heterocycles, and accordingly this study began with the targeted conversion of **1a** to **2a** (Table 1, Eq 1). While the precedent for the atroposelective cyclodehydration was initially focused on diastereoselectivity,[9] we commenced the comparative study by expanding this finding to an enantioselective method for atropisomer-selective synthesis of axially chiral benzimidazoles with both the pThr-type and C_2-type of CPA. We initially examined 19 pThr-type catalysts for the atropisoselective cyclization. Catalyst **P1** (with a canonical ^{D}Pro-Aib sequence at the i+1 and i+2 positions)[21] was evaluated to benchmark the catalyst-dependent enantioselectivity against a well-studied β-turn inducing peptide sequence resulting in product, **2a** with a 43% e.e. at 74% con-version (Table 1A, entry 1). Standard variations of the peptide sequence led to significant improvements. Essentially all residues transmit stereochemical information to the reaction coordinate, whether the individual residues are locally chiral or not.[22] While ex-tended commentary could be provided about the complete set, significant conclusions pointed to the critical nature of a ^{D}Pro residue at i+1 (Table 1A, entry 1 versus entry 2), as well as a synergistic advantage conferred by an aminocyclopropane carboxylic acid residue (Acpc; Table 1A, entries 4, 10–19) at the i+2 position, and a branched L-configured cyclohexylglycine residue (Chg; Table 1A, entries 15–19) at the i+3 residue. An N-terminal benzoyl group was also found to be optimal, such that catalyst **P19** was declared the lead catalyst, delivering **2a** with a 94% e.e. at 94% conversion (Table 1A, entry 19).[23]

In parallel, we asked exactly the same question with C_2-type CPAs. Shown in Table 1B are the results of atroposelective cyclodehydrations with 14 variously substituted common BINOL-derived CPAs. Notably, the results, from a purely enantioselectivity-centric per-

spective are comparable to the results obtained with the pThr-type catalysts. For example, *p*-substituted catalysts **B1** and **B2** provide a modest level of initial selectivity at good conversion (58% e.e. and 52% e.e., respectively; Table 1B, entries 1 and 2). *o*-Substitution with **B3**, **B4**, and **B5** leads to improvement, with up to 89% e.e. (Table 1B, entries 3–5). Apparent electronic effects also emerged, as the *m*-substituted catalysts **B6**, **B7**, and **B8** gave a range of results (Table 1B, entries 6–8), with **B9**, the *m,m*-diphenyl substituted catalyst, giving 89% e.e. in excellent conversion (Table 1B, entry 9). Further substitution leveraged apparent combinations of various features (*vide infra*). Tris-substitution on the BINOL-aryl substituent gave a set of catalysts that were quite effective for the atropoisomer-selective cyclodehydration, as **B10**–**13** all converged to give **2a** with between 90% and 92% e.e. for the canonical TRIP catalyst[24] (Table 1B, entries 10–13). Catalyst **B14** bearing 9-anthracenyl groups afforded the highest selectivity observed, delivering **2a** with 96% e.e. at full conversion (Table 1B, entry 14).

Substrate evaluation.

From these optimization studies a ques-tion arises: is the privileged C_2-symmetric type catalyst **B14** (96% e.e., 100% conversion) clearly better than peptidic catalyst **P19** (94% e.e., 97% conversion)? Analysis of each against a panel of 22 systematically modified substrates allows a data-driven inquisition (Figure 2). Noteworthy, cyclodehydrations procced efficiently with both catalysts, while moderate conversions were observed with sterically congested *o,o'*-disubstituted substrates.[23] We first evaluated three additional 6-substituted substrates, **2b**–**d** (Figure 2a). Removing the remote ^{t}Bu group (i.e., **1b** to **2b**) impacted enantioselectivity, as both **P19** and **B14** process this substrate with a slightly lower level of selectivity (**P19**, 91% e.e., **B14**, 88% e.e.). An electron donating group also leads to a slight drop in selectivity for both catalysts (**P19**, 92% e.e.; **B14**, 94% e.e.), while an electron withdrawing group enhances the asymmetric catalysis (**P19**, 97% e.e.; **B14**, 97% e.e.). But, most noteworthy is that **P19** and **B14** are all but indistinguishable with these substrates. Substitution at the 7-position, however, cre-ates an entirely different scenario. For five different substrates (**1e**–**i**), peptidic catalyst **P19** appears to offer more generality, as benzimidazoles **2e**–**i** are delivered with 89–93% e.e. for this class (Figure 2b). In contrast, C_2-type catalyst **B14** seems poorly suited to these substrates, as the products are obtained with 44–76% e.e. (**2e**–**h**), with the exception of **2i** being isolated with 83% e.e. (*cf.* 89% e.e. with **P19**). Several other substrates also reveal the differential attributes of pThr-type and C_2-type CPAs. For example, as shown in Figure 2c, substitution at the 5-position (*i.e.*, **2j**) is better tolerated with **P19** (94% e.e.) than with **B14** (90% e.e.). Incorporating differ-ent substitution patterns on the bottom arene of the diarylaniline moiety also reveals curious effects. Highly substituted axially chiral benzimidazoles **2k**–**m** (Figure 2d) are all formed with excellent enantioselectivity when either **P19** (93–97% e.e.) or **B14** (93–96% e.e.) are used as the catalysts. Exceptions appear in the formation of **2n** where **B14** (95% e.e.) is slightly more effective than **P19** (85% e.e.) and vice versa in the formation of **2o** (**P19**, 89% e.e.; **B14**, 88% e.e.). Some striking differences also emerge with *o,o'*-disubstituted substrates **2p**–**r** (Figure 2e). In these cases, low enantioselectivities are observed with both **P19** and **B14** as the catalyst. While **B14** pro-vides a somewhat higher enantioselectivity in the cases of **2p** and **2r**, neither catalyst gives promising results. However, when a second R-

group is added to the remote arene, as in the case **2s** and **2t**, quite good enantioselectivities are recorded by both catalysts. Benzannu-lated analogue (**2u**) is slightly better accommodated with **P19** (94% e.e.) than with **B14** (91% e.e.). Yet, both **P19** and **B14** are poor catalysts for the formation of **2v**, with a basic *N*-atom introduced re-mote from the loci of bond formation (Figure 2i, 16% e.e. and 2% e.e., respectively). The absolute configuration of **2a** was determined by X-ray crystallographic analysis after recrystallization (Figure 2j), and those of other products in Figure 2 were displayed by analogy.

Mechanistic experiments for P19.

As a synthetic method, per-haps most would agree that **P19** and **B14** are promising new tools for an underexplored area of enantioselective catalysis. However, what do their similarities and differences in performance tell us about their respective mode of stereoinduction? For this question, we turned to mechanistic studies. The manner in which one can in-terrogate the mechanistic details of **P19** and **B14** is different.

Computation, particularly at the DFT level, has emerged as a pow-erful tool for assessing the feasibility of mechanistic steps involved in catalysis and the origins of enantioinduction.[25] These techniques are renowned for the interrogation of rigid C_2-type catalysts like **B1**–**14**. In contrast, peptide-based catalysts like **P19** present special challenges, and computational analyses of such flexible systems are far from routine.[26] The complication arises from the many plausible ground state (GS) and transition state (TS) conformations, which require exhaustive sampling and may require molecular dynamic simulations for effective conformation generation, an inherently time consuming process.[27] A range of experimental techniques, however, offers a complementary way to probe the effect of the catalyst structure on enantioselectivity, and in some instances are faster to complete than computations. In this regard, we performed two types of studies including, (a) evaluation of catalyst analogs, and (b) investigation of the catalyst structure by NMR techniques. For the former, truncated peptides **P20**–**22** were prepared and evaluated to isolate the minimal determinants of selectivity and striking results were obtained (Figure 3a). To begin, phosphorylated threonine monomer, **P20**, shows moderate enantioselectivity favoring the enantiomeric product of **2a**, suggesting that the high enantioselectivity of **P19** is not dominated by the local stereoconfiguration of threonine, but ra-ther on the global conformation of the peptide.[28] Elongation to the dipeptide (*i.e.*, **P21**) also affords *ent*-**2a** as a major enantiomer (−42% e.e.), while the tripeptide **P22** gives almost racemic mixture of **2a**. High enantioselectivity was only observed with the Fmoc protected tetrapeptide, **P15**.

These results also imply additional non-covalent interactions be-tween the cyclohexyl group at *i*+3 residue and **1a** and/or considerable conformational changes induced by the introduction of *i*+3 residue. For direct observation of the catalyst structure, ^{1}H−^{1}H ROESY NMR studies of **P19** were performed. We observed 15 non-sequential ROE correlations as shown in Figure 3b. Contacts (red arrows) of N−H_{acpc} with the bottom face of ^{D}Pro and the proton of the αC-H of pThr suggest that the N−H bond is likely located underneath the ^{D}Pro residue, in proximity to potential hydrogen bond acceptors C=O_{Thr} and C=O_{Bz}. Considering ROE contacts (blue arrows) of the cyclohexyl group with the protons of C−H of ^{D}Pro and βC-H of Thr, a β-turn conformation appears supported by the hydrogen bond be-tween N–

H_{chg} and $C{=}O_{Thr}$ as shown in Figure 3c. Multiple correlations (green arrows in Figure 3b) between the dimethylamide at the C-terminus and benzylic and aromatic protons of -OBn/-NHBz of pThr are consistent with our hypothetical conformation and also in-dicate that the *i* +3 residue would be in proximity with the phosphoric acid. Given the steric effect of the *i*+3 residue as described in Table 1A, secondary interaction between the cyclohexyl group and substrate may have a beneficial influence on atroposelectivity.

DFT calculations for B14.

In evaluating the mechanism of C_2-type catalysts like **B14**, DFT and experimental results strongly suggest that cyclization is both rate and enantiodetermining.[23] To probe the origins of enantioinduction, we performed geometry optimizations with ωB97XD/6–31G(d) followed by single-point calculations at the ωB97XD/6–31G(d,p) level in toluene with the polarizable continuum model, IEFPCM using optimal catalyst **B14** containing an anthryl group. The calculations corroborate the magnitude (exp. 96% e.e., calc. 93% e.e.) and sense of enantioinduction (Figure 4a). The key controlling element appears to be a steric interaction be-tween the naphthyl group on the substrate and the 3,3′ substituents on the catalyst (Figure 4a). To precisely explore the contributions of the *t*-butyl and the naphthyl substituents on the substrate structure to the TS energies, two truncation studies were performed computationally. Firstly, the *t*-butyl substituent was replaced for a proton and a single-point energy was taken of the resulting structures without re-optimization.[29] The energy difference ($\Delta\Delta E^{\ddagger}$) between the competing structures increased from 2.4 to 4.0 kcal mol^{-1}, which suggests that the *t*-butyl group is not a major element in the catalyst-substrate interactions. However, replacing the naphthyl group for a phenyl group led to a significant decrease in $\Delta\Delta E^{\ddagger}$ from 2.4 to 0.8 kcal mol^{-1}. These truncation studies are consistent with the primary determinants of enantioselectivity being the interactions between the 3,3′ substituents on the catalyst and the naphthyl substituent of the substrate. Further interrogation of the mechanistic basis for the selectivity afforded by C_2-type catalysts was accomplished using statistical comparison of catalysts substituent changes to reaction enantioselectivity (expressed as $G^{\ddagger}$).[30] Collected parameters for the correlations included IR vibrational frequencies and intensities, torsion angles, NBO charges and Sterimol steric descriptors (L, B1, B5). A simple model prioritizes steric effects measured though torsion and two other terms: the $P{=}O_{as}$ stretch likely describing H-bond contacts and the cross term $*B1_{C3}$, a steric correction for the inclusion of 9-anthryl, as additional selectivity discriminants.

Comprehensive model and determinants.

Perhaps the most powerful analysis of the differences between the two catalyst classes can be achieved by using a substrate profiling technique wherein the performance of each catalyst is analyzed through correlation of substrate outcomes. Specifically, we anticipated that the subtle differences in substrate performance as a function of catalyst class could be related through overlapping and varying sensitivities to the substrate, providing insight into how these catalysts induce stereoselectivity. We hypothesized that **2a**–**t** offered the requisite changes to both the electronic and steric environments of the substrate (Figure 5) but also incorporates sufficient overlapping features for analysis.

To define the parameter library, DFT optimizations were per-formed on these substrates at the M06–2X/def2-TZVP level of the-ory wherein NBO charges, IR vibrations and Sterimol values were collected to probe structural effects.[31] A statistical model consisting of four terms was determined for the BINOL-derived phosphoric acids. The included parameters suggest that the process proceeds via a TS that minimizes steric repulsions between the large 3,3′ groups on the catalyst and the substrate (Figure 5a), which is consistent with both the DFT and catalyst correlation studies detailed above. For example, the negative coefficient with the L_{C7} term describes likely repulsive interactions in TS_{Re} with the C_7 substituent and the 3,3′ substituents. The terms $B5_{C6}$ and the $B1_{ortho}$ both describe the preferred orientation of the bottom ring in the TS. Reducing the size of the substituent at C_6 decreases the repulsion between the top and the bottom rings in the cyclization step. In this case, the more compact, the third TS, in which the larger substituent on the bottom aromatic ring points towards the top aromatic ring (second TS structure in Figure 5b), would be more plausible leading to decreased enantioselectivity. Complementary to the catalyst statistical model (Figure 4b and 5a), the NBO_O term is likely describing H-bond contacts between the catalyst and substrate.

Intriguingly, the pThr-type catalysts counterparts do not function through an analogous model of enantioinduction, despite the same catalytic apparatus for bond formation (i.e., the CPA moiety itself). For the pThr-type catalysts, the mathematical model consists of three conserved terms. Two of these terms essentially describe the bottom ring orientation preferences, an apparent locus of critical catalyst-substrate interactions. The NBO term is likely indicative of the hydrogen bonding features of phosphoric acid with the substrate. However, most notably, the peptide system does not include an additional penalizing steric term in the model. Despite steric effects and the proximity of the *i*+3 residue to the phosphoric acid as observed in Table 1A and Figure 3, this catalyst class still provides an alternative mode of enantioinduction. This effect may be consistent with the enhanced generality in scope for substrate variation in this vicinity; the flexible peptide system may also be adaptive to substrate steric demands, as is evidenced in other peptide-based catalysts.[26,27] Comparison of the magnitudes of the coefficient terms can provide further insight into the stereocontrolling elements responsible for enantioinduction. Intriguingly, the $B5_{C6}$ term is statistically more significant for the C_2-type CPAs. This suggests that due to steric repulsion between the catalyst 3,3′ substituents and the bottom aromatic ring of the substrate that a compact arrangement may be more readily favored. The proposed physical meaning behind each of the terms in the mathematical equations have been summarized in Figure 5b.

CONCLUSIONS

Although the general principles of energetic differentiation underlying asymmetric catalysis by distinct catalyst families are essentially the same, significant mechanistic differences can lead to similar selectivity outcomes. Fundamentally, destabilizing effects and stabilizing noncovalent interactions of a variety of types can all contribute to the differential energies of competing transition states within an ensemble. In the present study, steric effects from reasonably large groups on both the catalyst and substrate appear to dictate enantioselectivity for C_2-type CPAs. In contrast, pThr-type CPAs appear to work through an

alternative mode of enantioinduction, where conformational adaptation presumably limits repulsive interactions. These experimental and computational findings allow us to revisit some of the questions posed in our introduction. For example, it seems ever clearer that various catalyst types may be found to achieve high levels of enantioselectivity for a given transformation of interest, and that if the mode of activation is general (e.g., Lewis/Brønsted acid activation, bifunctional catalysis, etc.), application to other reactions with mechanistic similarity can follow. Yet, the redundancy of mechanistic solutions to common overall transformations may expand the concept of the privileged catalyst. In this sense, as the field evolves, it seems there may be less privilege, indeed less uniqueness of solution, as more catalyst types are discovered for a given type of enantioselectivity transformation. The expanded array of catalyst available also enables exploration of ever-expanding substrate space. Accordingly, new layers of mechanistic complexity are introduced when unusual substrate types are evaluated. Therein, situations emerge where catalyst functional equivalences may be lifted. In such situations, mechanistic complementarity among catalyst types may be particularly critical for broad spectrum success with highly diverse substrates. And of course, these same issues will likely emerge as each catalyst type is profiled in an ever-expanding list of reaction types. In this sense, a case may exist for an ever expanding, perhaps less privileged catalyst catalog, placing a premium on catalytic structural diversity and diverse catalytic mechanisms that control secondary, outer sphere interactions. This is a hallmark of enzymatic catalysis, where diversity of function on common catalyst scaffolds has emerged alongside an impressive array of catalyst specificities.[32]

Supplementary Material

Refer to Web version on PubMed Central for supplementary material.

ACKNOWLEDGMENT

M.S.S., F.D.T., and S.J.M. are grateful to the National Institute of General Medical Sciences of the National Institutes of Health for support (GM-121383). The authors are grateful to Christopher R. Shugrue, Aaron L. Featherston and Dr. Anthony J. Metrano for preparation of catalysts and helpful discussions. We also would like to thank Dr. Brandon Q. Mercado for solving our X-ray crystal structures. J.M.C. acknowledges the support of the NSF Graduate Research Fellowship Program. Computational resources were provided by the Center for High Performance Computing at the University of Utah and the Extreme Science and Engineering Discovery Environment (XSEDE), which is supported by the NSF (ACI-1548562).

REFERENCES

1. Jacobsen EN; Pfaltz A; Yamamoto H, Comprehensive Asymmetric Catalysis I-III.: Suppl. I-II Springer: Berlin/Heidelberg, 1999.
2. Yamamoto H; Carreira EM, Comprehensive Chirality Elsevier Science: Amsterdam, 2012.
3. a Canali L; Sherrington C, D., Utilisation of homogeneous and supported chiral metal(salen) complexes in asymmetric catalysis. Chem. Soc. Rev 1999, 28, 85–93(b)Helmchen G; Pfaltz A, PhosphinooxazolinesA New Class of Versatile, Modular P,N-Ligands for Asymmetric Catalysis. Acc. Chem. Res 2000, 33, 336–345 [PubMed: 10891051] (c)Noyori R; Takaya H, BINAP: an efficient chiral element for asymmetric catalysis. Acc. Chem. Res 1990, 23, 345–350.
4. Yoon TP; Jacobsen EN, Privileged Chiral Catalysts. Science 2003, 299, 1691–1693. [PubMed: 12637734]
5. Zhou QL, Privileged Chiral Ligands and Catalysts Wiley: 2011.

6. (a) Burk MJ; Feaster JE; Nugent WA; Harlow RL, Preparation and use of C2-symmetric bis(phospholanes): production of .alpha.-amino acid derivatives via highly enantioselective hydrogenation reactions. J. Am. Chem. Soc 1993, 115, 10125–10138(b)Junge K; Oehme G; Monsees A; Riermeier T; Dingerdissen U; Beller M, Synthesis of new chiral monodentate phosphines and their use in asymmetric hydrogenation. Tetrahedron Lett 2002, 43, 4977–4980(c)Knowles WS; Sabacky MJ; Vineyard BD, Catalytic asymmetric hydrogenation. J. Chem. Soc., Chem. Commun 1972, 10–11(d)Togni A; Breutel C; Schnyder A; Spindler F; Landert H; Tijani A, A Novel Easily Accessible Chiral Ferrocenyldiphosphine for Highly Enantioselective Hydrogenation, Allylic Alkylation, and Hydroboration Reactions. J. Am. Chem. Soc 1994, 116, 4062–4066.
7. (a) Sakthivel K; Notz W; Bui T; Barbas CF, Amino Acid Catalyzed Direct Asymmetric Aldol Reactions: A Bioorganic Approach to Catalytic Asymmetric Carbon–Carbon Bond-Forming Reactions. J. Am. Chem. Soc 2001, 123, 5260–5267 [PubMed: 11457388] (b)Tang Z; Jiang F; Yu L-T; Cui X; Gong L-Z; Mi A-Q; Jiang Y-Z; Wu Y-D, Novel Small Organic Molecules for a Highly Enantioselective Direct Aldol Reaction. J. Am. Chem. Soc 2003, 125, 5262–5263 [PubMed: 12720423] (c)Kano T; Takai J; Tokuda O; Maruoka K, Design of an Axially Chiral Amino Acid with a Binaphthyl Backbone as an Organocatalyst for a Direct Asymmetric Aldol Reaction. Angew. Chem. Int. Ed 2005, 44, 3055–3057(d)Zheng B-L; Liu Q-Z; Guo C-S; Wang X-L; He L, Highly enantioselective direct aldol reaction catalyzed by cinchona derived primary amines. Org. Biomol. Chem 2007, 5, 2913–2915 [PubMed: 17728855] (e)Trost BM; Brindle CS, The direct catalytic asymmetric aldol reaction. Chem. Soc. Rev 2010, 39, 1600–1632. [PubMed: 20419212]
8. (a) Ishihara K; Yamamoto H, Bronsted Acid Assisted Chiral Lewis Acid (BLA) Catalyst for Asymmetric Diels-Alder Reaction. J. Am. Chem. Soc 1994, 116, 1561–1562(b)Evans DA; Murry JA; von Matt P; Norcross RD; Miller SJ, C2-Symmetric Cationic Copper(II) Complexes as Chiral Lewis Acids: Counterion Effects in the Enantioselective Diels–Alder Reaction. Angewandte Chemie International Edition in English 1995, 34, 798–800(c)Corey EJ; Shibata T; Lee TW, Asymmetric Diels—Alder Reactions Catalyzed by a Triflic Acid Activated Chiral Oxazaborolidine. J. Am. Chem. Soc 2002, 124, 3808–3809 [PubMed: 11942799] (d)Ma S, Asymmetric catalysis of Diels-Alder reaction in Handbook of cyclization reactions, Vol. 1 Wiley-VCH: Weinheim, 2010.
9. Kwon Y; Chinn AJ; Kim B; Miller SJ, Divergent Control of Point and Axial Stereogenicity: Catalytic Enantioselective C—N Bond-Forming Cross-Coupling and Catalyst-Controlled Atroposelective Cyclodehydration. Angew. Chem. Int. Ed 2018, 57, 6251–6255.
10. Taylor RD; MacCoss M; Lawson ADG, Rings in Drugs. J. Med. Chem 2014, 57, 5845–5859. [PubMed: 24471928]
11. (a) Akiyama T; Itoh J; Yokota K; Fuchibe K, Enantioselective Mannich-Type Reaction Catalyzed by a Chiral Brønsted Acid. Angew. Chem. Int. Ed 2004, 43, 1566–1568(b)Uraguchi D; Terada M, Chiral Brønsted Acid-Catalyzed Direct Mannich Reactions via Electrophilic Activation. J. Am. Chem. Soc 2004, 126, 5356–5357. [PubMed: 15113196]
12. (a) Parmar D; Sugiono E; Raja S; Rueping M, Complete Field Guide to Asymmetric BINOL-Phosphate Derived Brønsted Acid and Metal Catalysis: History and Classification by Mode of Activation; Brønsted Acidity, Hydrogen Bonding, Ion Pairing, and Metal Phosphates. Chem. Rev 2014, 114, 9047–9153 [PubMed: 25203602] (b)Maji R; Mallojjala SC; Wheeler SE, Chiral phosphoric acid catalysis: from numbers to insights. Chem. Soc. Rev 2018, 47, 1142–1158. [PubMed: 29355873]
13. Manning BD; Cantley LC, AKT/PKB Signaling: Navigating Downstream. Cell 2007, 129, 1261–1274. [PubMed: 17604717]
14. (a) Rueping M; Antonchick AP; Theissmann T, A Highly Enantioselective Brønsted Acid Catalyzed Cascade Reaction: Organocatalytic Transfer Hydrogenation of Quinolines and their Application in the Synthesis of Alkaloids. Angew. Chem. Int. Ed 2006, 45, 3683–3686(b)Shugrue CR; Miller SJ, Phosphothreonine as a Catalytic Residue in Peptide-Mediated Asymmetric Transfer Hydrogenations of 8-Aminoquinolines. Angew. Chem. Int. Ed 2015, 54, 11173–11176.
15. (a) Xu S; Wang Z; Zhang X; Zhang X; Ding K, Chiral Brønsted Acid Catalyzed Asymmetric Baeyer–Villiger Reaction of 3-Substituted Cyclobutanones by Using Aqueous H2O2. Angew. Chem. Int. Ed 2008, 47, 2840–2843(b)Featherston AL; Shugrue CR; Mercado BQ; Miller SJ, Phosphothreonine (pThr)-Based Multifunctional Peptide Catalysis for Asymmetric Baeyer–Villiger Oxidations of Cyclobutanones. ACS Catal 2019, 9, 242–252. [PubMed: 31007966]

16. Knowles RR; Jacobsen EN, Attractive noncovalent interactions in asymmetric catalysis: Links between enzymes and small molecule catalysts. Proc. Natl. Acad. Sci. U.S.A 2010, 107, 20678–20685. [PubMed: 20956302]

17. (a)For selected reviews, see: Wang Y-B; Tan B, Construction of Axially Chiral Compounds via Asymmetric Organocatalysis. Acc. Chem. Res 2018, 51, 534–547 [PubMed: 29419282] (b)Bringmann G; Gulder T; Gulder TAM; Breuning M, Atroposelective Total Synthesis of Axially Chiral Biaryl Natural Products. Chem. Rev 2011, 111, 563–639 [PubMed: 20939606] (c)Ma G; Sibi MP, Catalytic Kinetic Resolution of Biaryl Compounds. Chem. Eur. J 2015, 21, 11644–11657. [PubMed: 26237330]

18. (a)For recent examples involving chiral phosphoric acids, see: Mori K; Ichikawa Y; Kobayashi M; Shibata Y; Yamanaka M; Akiyama T, Enantioselective Synthesis of Multisubstituted Biaryl Skeleton by Chiral Phosphoric Acid Catalyzed Desymmetrization/Kinetic Resolution Sequence. J. Am. Chem. Soc 2013, 135, 3964–3970 [PubMed: 23413828] (b)Min C; Lin Y; Seidel D, Catalytic Enantioselective Synthesis of Mariline A and Related Isoindolinones through a Biomimetic Approach. Angew. Chem. Int. Ed 2017, 56, 15353–15357(c)Zhang L; Zhang J; Ma J; Cheng D-J; Tan B, Highly Atroposelective Synthesis of Arylpyrroles by Catalytic Asymmetric Paal–Knorr Reaction. J. Am. Chem. Soc 2017, 139, 1714–1717 [PubMed: 28106384] (d)Chen Y-H; Qi L-W; Fang F; Tan B, Organocatalytic Atroposelective Arylation of 2-Naphthylamines as a Practical Approach to Axially Chiral Biaryl Amino Alcohols. Angew. Chem. Int. Ed 2017, 56, 16308–16312.

19. Cherney AH; Kadunce NT; Reisman SE, Enantioselective and Enantiospecific Transition-Metal-Catalyzed Cross-Coupling Reactions of Organometallic Reagents To Construct C–C Bonds. Chem. Rev 2015, 115, 9587–9652. [PubMed: 26268813]

20. (a) Gustafson JL; Lim D; Miller SJ, Dynamic Kinetic Resolution of Biaryl Atropisomers via Peptide-Catalyzed Asymmetric Bromination. Science 2010, 328, 1251–1255 [PubMed: 20522769] (b)Bhat V; Wang S; Stoltz BM; Virgil SC, Asymmetric Synthesis of QUINAP via Dynamic Kinetic Resolution. J. Am. Chem. Soc 2013, 135, 16829–16832 [PubMed: 24152221] (c)Mori K; Itakura T; Akiyama T, Enantiodivergent Atroposelective Synthesis of Chiral Biaryls by Asymmetric Transfer Hydrogenation: Chiral Phosphoric Acid Catalyzed Dynamic Kinetic Resolution. Angew. Chem. Int. Ed 2016, 55, 11642–11646.

21. Metrano AJ; Abascal NC; Mercado BQ; Paulson EK; Hurtley AE; Miller SJ, Diversity of Secondary Structure in Catalytic Peptides with β-Turn-Biased Sequences. J. Am. Chem. Soc 2017, 139, 492–516. [PubMed: 28029251]

22. Hurtley AE; Stone EA; Metrano AJ; Miller SJ, Desymmetrization of Diarylmethylamido Bis(phenols) through Peptide-Catalyzed Bromination: Enantiodivergence as a Consequence of a 2 amu Alteration at an Achiral Residue within the Catalyst. J. Org. Chem 2017, 82, 11326–11336. [PubMed: 29020446]

23. See the Supporting Information for details.

24. Seayad J; Seayad AM; List B, Catalytic Asymmetric Pictet—Spengler Reaction. J. Am. Chem. Soc 2006, 128, 1086–1087. [PubMed: 16433519]

25. Cheng G-J; Zhang X; Chung LW; Xu L; Wu Y-D, Computational Organic Chemistry: Bridging Theory and Experiment in Establishing the Mechanisms of Chemical Reactions. J. Am. Chem. Soc 2015, 137, 1706–1725. [PubMed: 25568962]

26. Crawford JM; Stone EA; Metrano AJ; Miller SJ; Sigman MS, Parameterization and Analysis of Peptide-Based Catalysts for the Atroposelective Bromination of 3-Arylquinazolin-4(3H)-ones. J. Am. Chem. Soc 2018, 140, 868–871. [PubMed: 29300461]

27. Yan XC; Metrano AJ; Robertson MJ; Abascal NC; Tirado-Rives J; Miller SJ; Jorgensen WL, Molecular Dynamics Simulations of a Conformationally Mobile Peptide-Based Catalyst for Atroposelective Bromination. ACS Catal 2018, 8, 9968–9979. [PubMed: 30687577]

28. Diener ME; Metrano AJ; Kusano S; Miller SJ, Enantioselective Synthesis of 3-Arylquinazolin-4(3H)-ones via Peptide-Catalyzed Atroposelective Bromination. J. Am. Chem. Soc 2015, 137, 12369–12377. [PubMed: 26343278]

29. These results cannot be transferred to rationalize or predict the catalyst/substrate performances, because the resulting structures are not optimized.

30. Orlandi M; Hilton MJ; Yamamoto E; Toste FD; Sigman MS, Mechanistic Investigations of the Pd(0)-Catalyzed Enantioselective 1,1-Diarylation of Benzyl Acrylates. J. Am. Chem. Soc 2017, 139, 12688–12695. [PubMed: 28800230]

31. (a) Sigman MS; Harper KC; Bess EN; Milo A, The Development of Multidimensional Analysis Tools for Asymmetric Catalysis and Beyond. Acc. Chem. Res 2016, 49, 1292–1301 [PubMed: 27220055] (b)Santiago CB; Guo J-Y; Sigman MS, Predictive and mechanistic multivariate linear regression models for reaction development. Chem. Sci 2018, 9, 2398–2412 [PubMed: 29719711] (c)Reid JP; Sigman MS, Comparing quantitative prediction methods for the discovery of small-molecule chiral catalysts. Nat. Rev. Chem 2018, 2, 290–305.

32. Anantharaman V; Aravind L; Koonin EV, Emergence of diverse biochemical activities in evolutionarily conserved structural scaffolds of proteins. Curr. Opin. Chem. Biol 2003, 7, 12–20. [PubMed: 12547421]

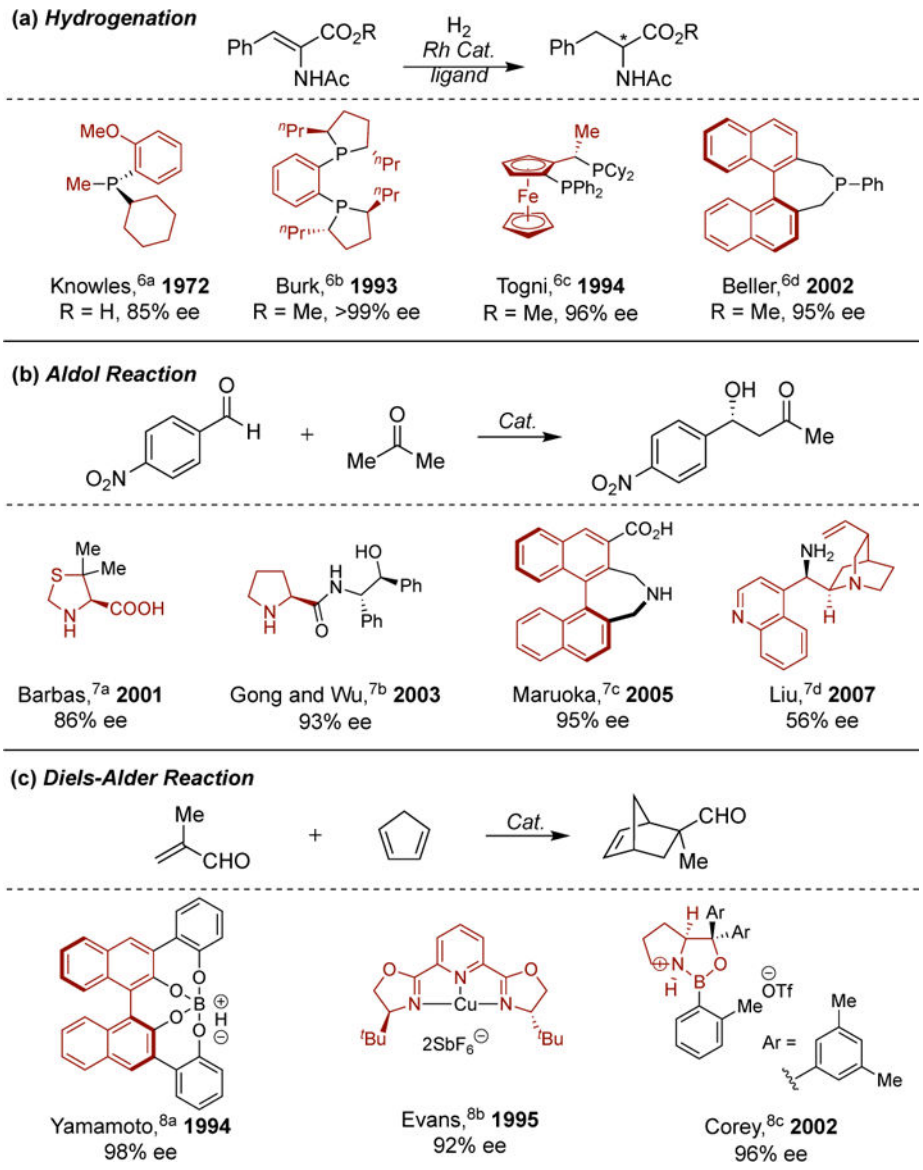

Scheme 1.

Selected Examples of Asymmetric Reactions that In-volve Same Substrate with Different Chiral Catalysts

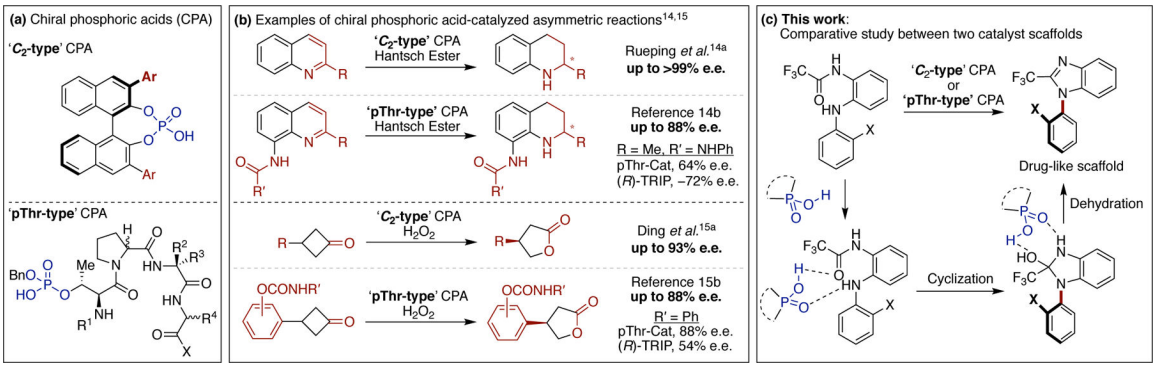

Figure 1.

(a) Chemical structures of 'C_2-type' CPA and 'pThr-type' CPA (b) Examples of chiral phosphoric acid-catalyzed asymmetric reactions (Top: Asymmetric transfer hydrogenation, Bottom: Asymmetric Baeyer-Villiger oxidation). (c) Atroposelective cyclodehydrations.

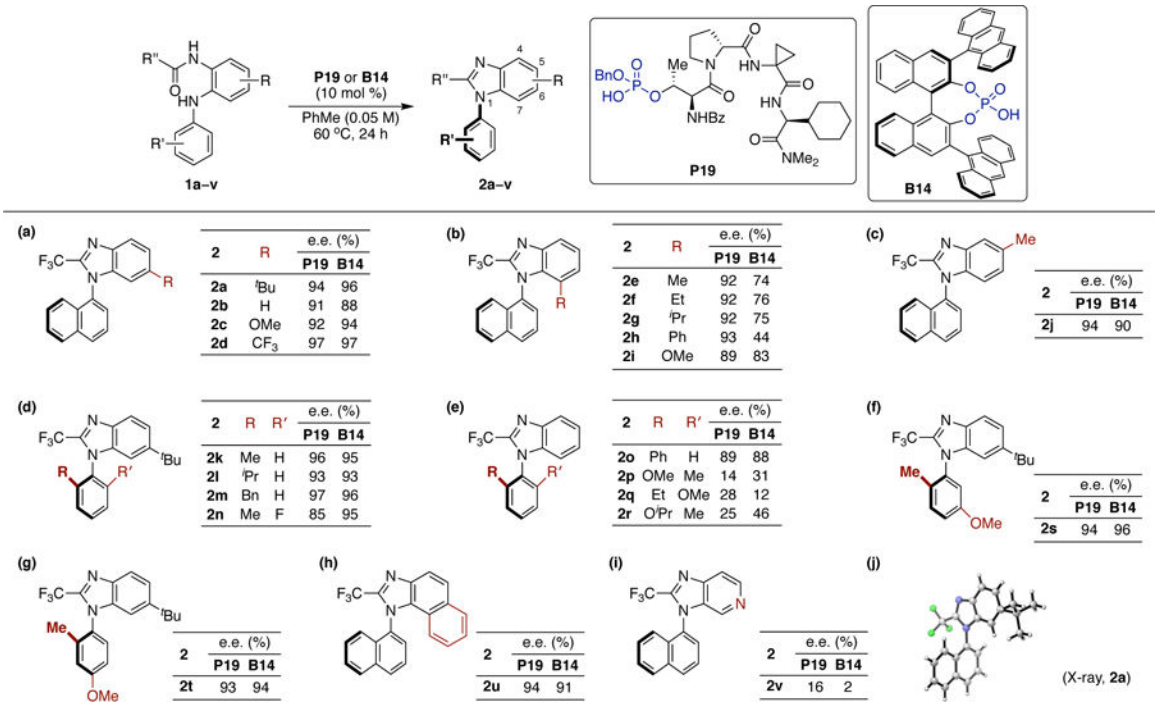

2	R	e.e. (%) P19	B14
2a	^{t}Bu	94	96
2b	H	91	88
2c	OMe	92	94
2d	CF_3	97	97

2	R	e.e. (%) P19	B14
2e	Me	92	74
2f	Et	92	76
2g	^{i}Pr	92	75
2h	Ph	93	44
2i	OMe	89	83

2	e.e. (%) P19	B14
2j	94	90

2	R	R′	e.e. (%) P19	B14
2k	Me	H	96	95
2l	^{i}Pr	H	93	93
2m	Bn	H	97	96
2n	Me	F	85	95

2	R	R′	e.e. (%) P19	B14
2o	Ph	H	89	88
2p	OMe	Me	14	31
2q	Et	OMe	28	12
2r	O^{i}Pr	Me	25	46

2	e.e. (%) P19	B14
2s	94	96

2	e.e. (%) P19	B14
2t	93	94

2	e.e. (%) P19	B14
2u	94	91

2	e.e. (%) P19	B14
2v	16	2

Figure 2.

Substrate scopes. Reported results are the average of two trials. Reaction conditions (unless otherwise noted): **1** (0.02 mmol), catalyst (**P19** or **B14**) (0.002 mmol, 10 mol %), PhMe (0.4 mL, 0.05 M), 60 °C, 24 h. Enantiomeric excesses were determined by chiral HPLC analysis. Absolute configuration of **2a** was determined by single-crystal X-ray diffraction analysis as shown in Figure 2j. All other absolute configurations were drawn based on analogy.

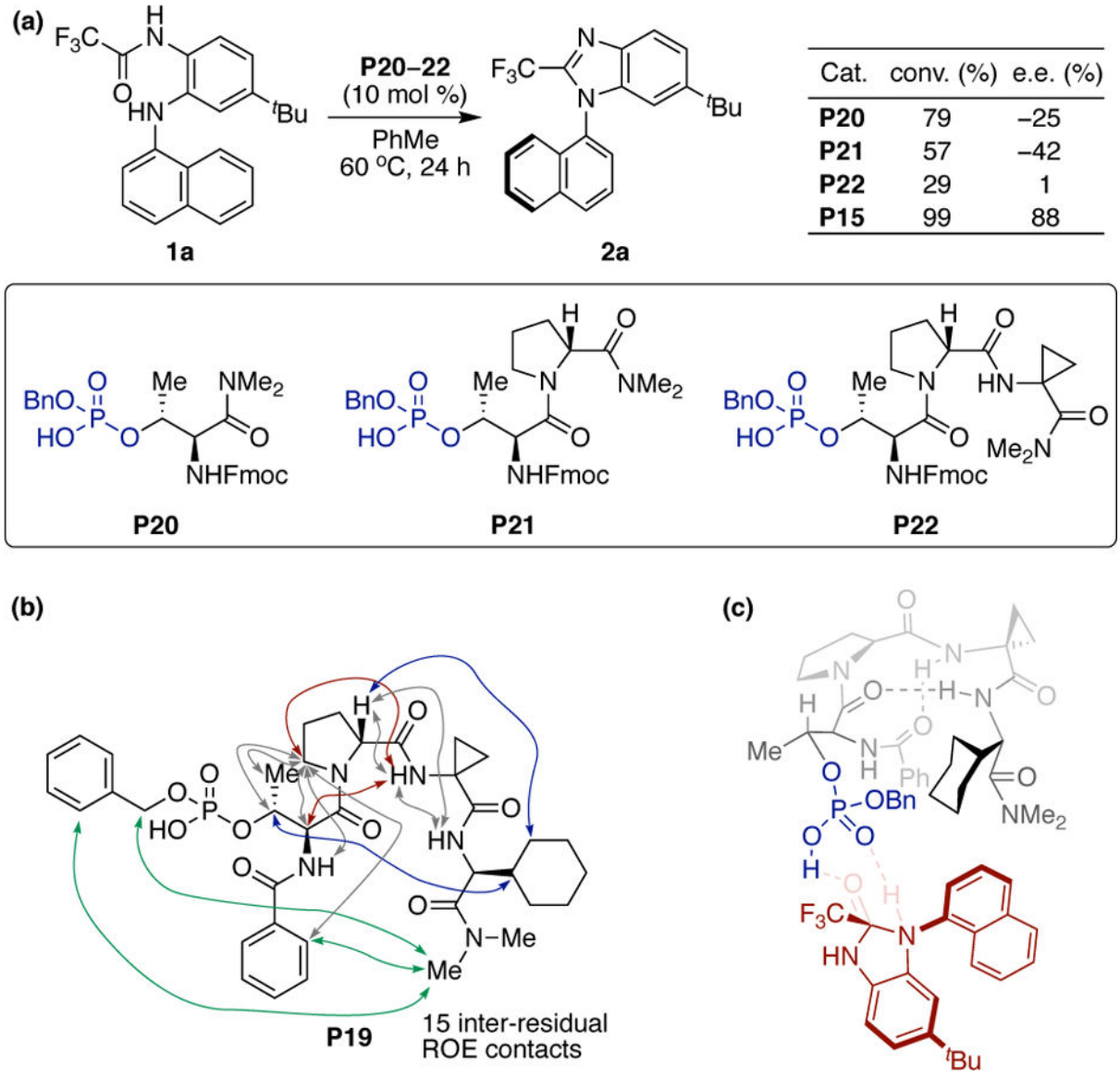

Cat.	conv. (%)	e.e. (%)
P20	79	−25
P21	57	−42
P22	29	1
P15	99	88

Figure 3.

(a) Truncation study of peptide catalyst. Reaction conditions (unless otherwise noted): **1a** (0.02 mmol), catalyst (**P20**–**22**) (0.002 mmol, 10 mol %), PhMe (0.2 mL, 0.1 M), 60 °C, 24 h. Conversions (as a percentage) were determined by ^{1}H NMR integrations of the aromatic peaks for the substrate and product. Enantiomeric excesses were determined by chiral HPLC analysis. (b) 15 inter-residue ROE contacts revealed by ^{1}H−^{1}H ROESY NMR of **P19**. (c) Proposed structure of **P19** and mechanistic model.

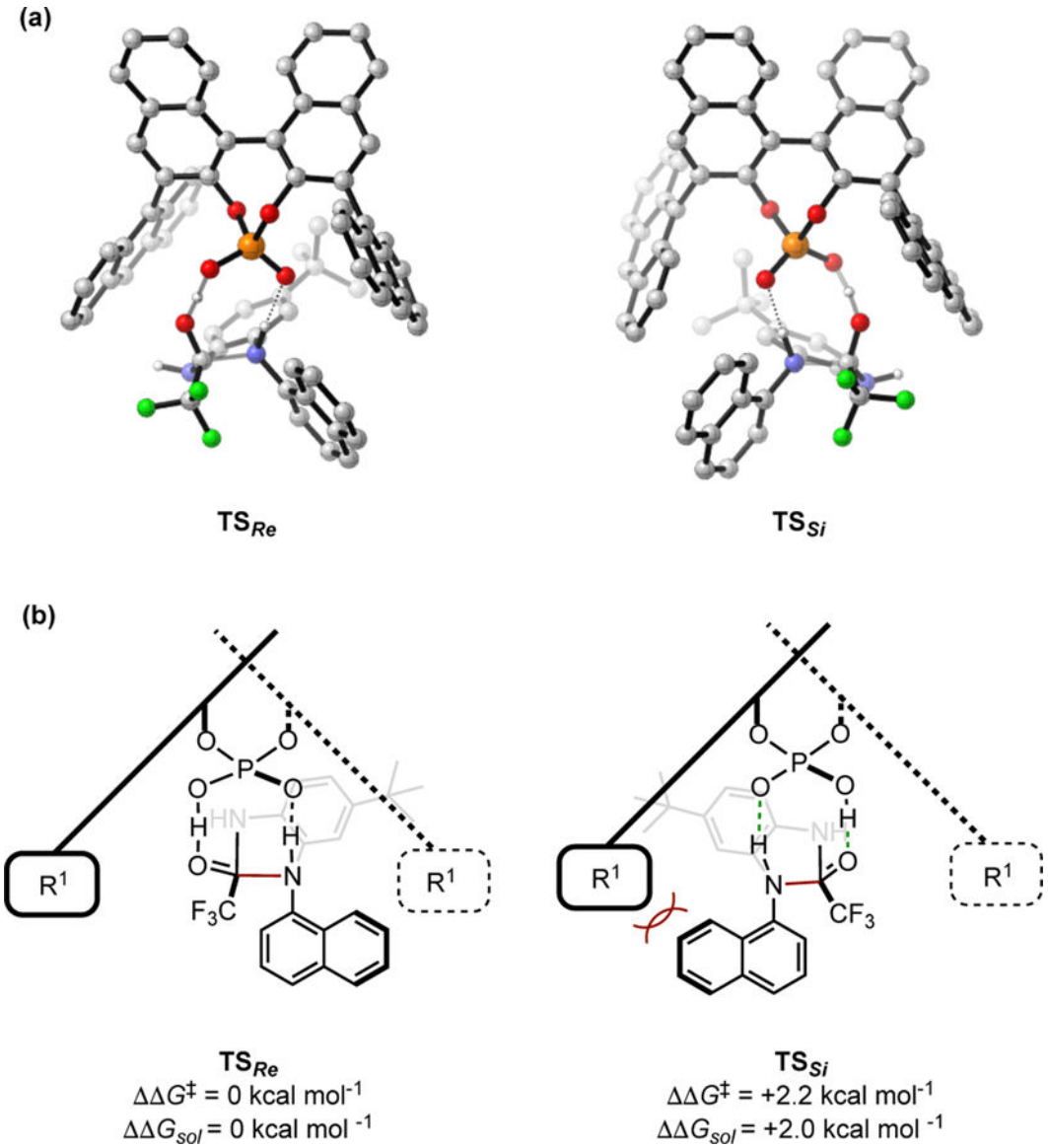

Figure 4.

(a) Cyclization TS calculated at ωB97XD/6–31G(d,p)-IEFPCM(toluene)//ωB97XD/6–31G(d) level of theory. Noncritical hydrogen atoms omitted for clarity. (b) Qualitative model describing the origins of enantioinduction. The repulsive steric interactions be-tween the naphthyl and the 3-substituent cause TS*Si* to be energetically disfavored. Reducing the size of the 3,3′ substituents reduces the interaction between them and would lead to lower e.e's.

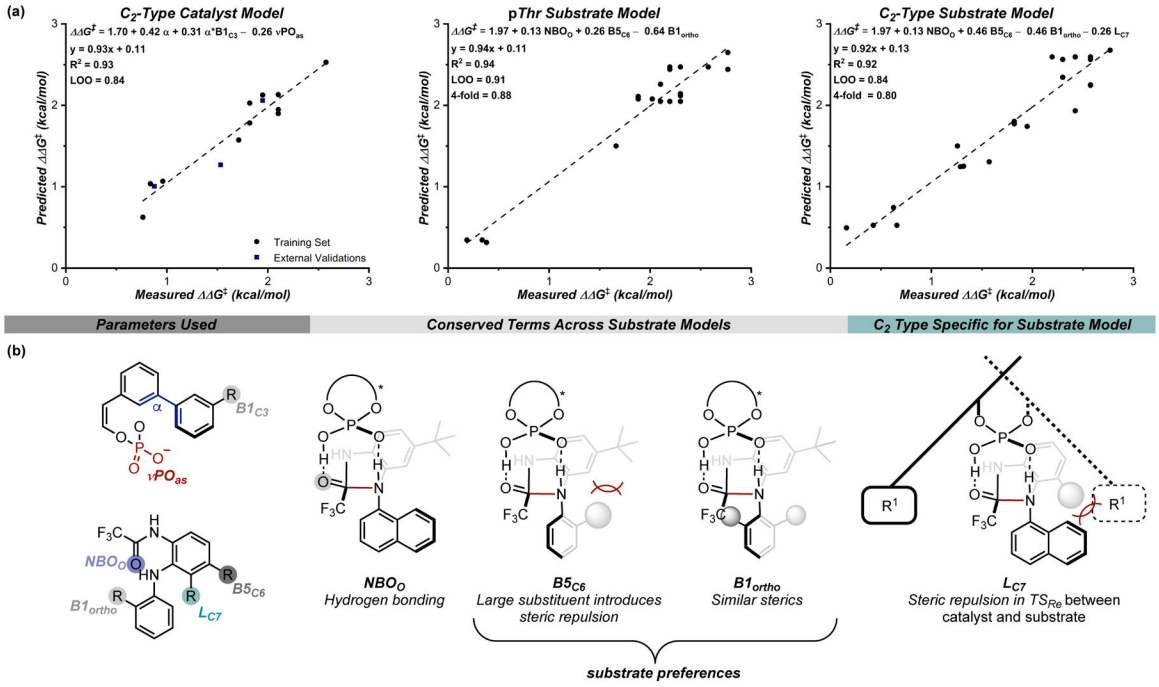

Figure 5.

(a) Evaluation of 3,3′-substituent features dictating enantioselectivity in the cyclodehydration reaction using an MLR model for a truncated C_2-type CPA (left) in addition to MLR models derived from substrate parameters for both the C_2-type CPA (center) and *p*Thr-type CPA (right). (b) Parameter assignments and MLR model deconstruction.

Table 1.

Catalyst Optimizations

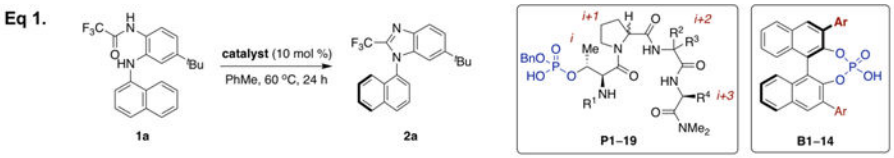

A. Peptide optimization

entry		catalyst *i*	*i*+1	*i*+2	*i*+3	Conv. (%)	e.e. (%)
1	**P1**	Fmoc-*p*Thr(Bn)	DPro	Aib	Phe-NMe_2	74	43
2	**P2**	Fmoc-*p*Thr(Bn)	LPro	Aib	Phe-NMe_2	23	1
3	**P3**	Fmoc-*p*Thr(Bn)	DPro	Gly	Phe-NMe_2	93	73
4	**P4**	Fmoc-*p*Thr(Bn)	DPro	Acpc	Phe-NMe_2	93	79
5	**P5**	Fmoc-*p*Thr(Bn)	DPro	Acbc	Phe-NMe_2	70	66
6	**P6**	Fmoc-*p*Thr(Bn)	DPro	Cle	Phe-NMe_2	67	53
7	**P7**	Fmoc-*p*Thr(Bn)	DPro	Aic	Phe-NMe_2	63	53
8	**P8**	Fmoc-*p*Thr(Bn)	DPro	Achc	Phe-NMe_2	71	50
9	**P9**	Fmoc-*p*Thr(Bn)	DPro	Phe	Phe-NMe_2	58	28
10	**P10**	Fmoc-*p*Thr(Bn)	DPro	Acpc	Gly-NMe_2	55	34
11	**P11**	Fmoc-*p*Thr(Bn)	DPro	Acpc	Ala-NMe_2	76	65
12	**P12**	Fmoc-*p*Thr(Bn)	DPro	Acpc	Phg-NMe_2	88	64
13	**P13**	Fmoc-*p*Thr(Bn)	DPro	Acpc	Leu-NMe_2	95	82
14	**P14**	Fmoc-*p*Thr(Bn)	DPro	Acpc	Tle-NMe_2	88	84
15	**P15**	Fmoc-*p*Thr(Bn)	DPro	Acpc	Chg-NMe_2	99	88
16	**P16**	Ac-*p*Thr(Bn)	DPro	Acpc	Chg-NMe_2	95	88
17	**P17**	4-OMe-Bz-*p*Thr(Bn)	DPro	Acpc	Chg-NMe_2	97	93
18	**P18**	4-NO_2-Bz-*p*Thr(Bn)	DPro	Acpc	Chg-NMe_2	100	89
19	**P19**	Bz-*p*Thr(Bn)	DPro	Acpc	Chg-NMe_2	97	94

B. 'C_2-type' catalyst optimization

entry	catalyst	Ar	Conv. (%)	e.e. (%)	entry	catalyst	Ar	Conv. (%)	e.e. (%)
1	**B1**		93	58	8	**B8**		70	86
2	**B2**		89	52	9	**B9**		96	89
3	**B3**		98	82	10	**B10**		100	92
4	**B4**		100	89	11	**B11**		100	90
5	**B5**		100	89	12	**B12**		100	91
6	**B6**		90	56	13	**B13**		100	92
7	**B7**		61	63	14	**B14**		100	96

Reaction conditions (unless otherwise noted): **1a** (0.02 mmol), catalyst (**P1**–**19** or **B1**–**14**) (0.002 mmol, 10 mol %), PhMe (0.2 mL, 0.1 M), 60°C, 24 h. Conversions (as a percentage) were determined by ^{1}H NMR integrations of the aromatic peaks for the substrate and product. Enantiomeric excesses were determined by chiral HPLC analysis. Abbreviations: Aib, 2-aminoisobutyric acid; Acpc, 1-aminocyclopropane carboxylic acid; Acbc, 1-aminocyclobutane carboxylic acid; Cle, cycloleucine (1-aminocyclopentane carboxylic acid); Aic, 2-aminoindane carboxylic acid; Achc, 1-aminocyclo-hexane carboxylic acid; Phg, phenylglycine; Tle, *tert*-Butylleucine; Chg, cyclohexylglycine.